Speckle statistics in OCT images: Monte Carlo simulations and experimental studies

Mikhail Yu. Kirillin,[1,2,*] Golnaz Farhat,[3,4] Ekaterina A. Sergeeva,[1] Michael C. Kolios,[5] and Alex Vitkin[2,3,6]

[1]*Institute of Applied Physics RAS, 603950, Ulyanov St., 46, Nizhny Novgorod, Russia*

[2]*Nizhny Novgorod State Medical Academy, 603005, Minin and Pozharsky Sq., 10/1, Nizhny Novgorod, Russia*

[3]*Department of Medical Biophysics, University of Toronto, 101 College Street, Room 15-701, Toronto, Ontario M5G 1L7, Canada*

[4]*Imaging Research, Sunnybrook Health Sciences Centre, 2075 Bayview Avenue, Toronto, Ontario M4N 3M5, Canada*

[5]*Department of Physics, Ryerson University, 350 Victoria Street, Toronto, Ontario M5B 2K3, Canada*

[6]*Department of Radiation Oncology, University of Toronto, 149 College Street, Suite 504, Toronto, Ontario M5T 1P5, Canada*

**Corresponding author: mkirillin@yandex.ru*

Received March 12, 2014; revised May 8, 2014; accepted May 8, 2014;
posted May 9, 2014 (Doc. ID 208143); published June 5, 2014

The speckle pattern of an optical coherence tomography (OCT) image carries potentially useful sample information that may assist in tissue characterization. Recent biomedical results *in vivo* indicate that the distribution of signal intensities within an OCT tissue image is well described by a log-normal-like (Gamma) function. To fully understand and exploit this finding, an OCT Monte Carlo model that accounts for speckle effects was developed. The resultant Monte Carlo speckle statistics predictions agree well with experimental OCT results from a series of control phantoms with variable scattering properties; the Gamma distribution provides a good fit to the theoretical and experimental results. The ability to quantify subresolution tissue features via OCT speckle analysis may prove useful in diagnostic photomedicine.

OCIS codes: (110.4500) Optical coherence tomography; (100.2960) Image analysis; (290.4210) Multiple scattering; (030.6140) Speckle.
http://dx.doi.org/10.1364/OL.39.003472

Optical coherence tomography (OCT) is a rapidly developing medical imaging technique being actively introduced into clinical practice. Based on the principles of low-coherence interferometry, OCT has been employed in ophthalmology where light scattering in the studied tissue layers is low, and thus image interpretation is relatively straightforward. Conversely, interpretation of OCT images in most other tissues often suffers from the confounding contribution of multiple scattering of the probing radiation within tissue. Besides blurring of tissue structural features in OCT images, strong scattering results in intensive overlapping of interference patterns produced by probing photons with similar optical path lengths. The phenomenon is manifest via a speckled structure of the OCT image, contributing to the difficulty of image interpretation. That said, the speckle structure of an OCT image is governed by optical properties of the imaged sample, namely, the local distribution of the backreflection coefficient; thus the analysis of speckle statistics can be employed for assessment of local tissue optical properties [1,2]. Such statistical analysis of OCT speckle pattern can potentially be automated, which may help in developing algorithms for pathology recognition, obviating the subjective and thus potentially unreliable evaluation by a physician. A number of recent publications are devoted to the development of such algorithms [3–7].

We employed an advanced Monte Carlo technique for simulation of OCT images based on our previously developed code [8,9]. A traditional approach to the simulation of an OCT signal [10] considers the distribution of the contributing photons that enter the OCT detection system over the range of simulated optical path lengths. In contrast, the key feature of our modeling approach is that the phase of each photon packet is tracked, and then the resultant OCT signal is calculated as a sum of fringe patterns originating from the interference of the individual photon packets with the reference beam [9]. This approach makes physical sense because the interference patterns are independent and hence additive. In the present study, we assume that probing radiation in the OCT system is randomly polarized, so the OCT signal (A-scan) for each transversal position of the probing beam can be written as [9,11]

$$I(z) = I_0 \sum_{i=1}^{N_{\mathrm{ph}}} \sqrt{W_i}\ \cos\left(\frac{2\pi}{\lambda}(2z - L_i)\right) \exp\left(-\left(\frac{2z - L_i}{l_c}\right)^2\right), \tag{1}$$

where I_0 is a constant defined by instrumental characteristics of the OCT system, N_{ph} is the total number of launched photon packets, W_i is the "conventional" MC weight of ith detected photon packet with optical path length L_i, $2z$ is the optical path length in the reference arm, and l_c is the coherence length of the light source. The shape of the coherence function of the source is assumed to be Gaussian, modeled by an exponential factor in Eq. (1). The simulated OCT detection system is described by two factors: the detector radius and the detecting aperture angle. The following setup parameters were used: a detecting aperture angle of 2°, probing beam (assumed Gaussian) with radius of 15 μm, and a detection aperture radius of 45 μm (100 μm above sample surface). One hundred consecutive A-scans with a transversal step of 10 μm were calculated in order to simulate an OCT B-mode image analogous to transverse scanning in an OCT system. For subsequent comparison with the experimental signal detection scheme, envelope detection of the simulated results was performed by filtering out the central (carrier) frequency.

A-scans and B-mode images were acquired using a custom-made swept-source OCT system similar to one described previously [12], based on a 36-facet polygon filter (Lincoln Laser Corp., Phoenix, Arizona). The system operates at a central wavelength of 1310 nm with in-air axial and lateral resolutions of 7.5 and 13.7 μm, respectively. As control samples with user-defined properties, we used aqueous suspensions of polystyrene ($n = 1.58$ at $\lambda = 1300$ nm) microspheres (Polysciences Inc. Warrington, Pennsylvania), with diameters of 0.35 and 0.5 μm and varying concentrations. The phantom properties were directly calculated using Mie scattering theory [13]. The optical properties of the microsphere suspensions were chosen in the range of physiological values and are summarized in Table 1.

We analyzed the speckle statistics by plotting the pixel intensities within selected ROIs of OCT B-mode scans using linear (not log-compressed) OCT signals. We have previously shown in *in vitro* cell samples [14] and in *in vivo* normal and tumor tissues [15] that the resultant signal intensity histogram distributions are well described by the Gamma and/or generalized Gamma distributions. This analysis draws upon analogous tissue characterization work in high-frequency ultrasound, whereby the resultant generalized Gamma distribution fitting parameters are given physical interpretation related to the average scatterer cross section, spatial distribution, and number density [16]. Such an interpretation currently lacks a physical basis in OCT and will be pursued in a separate future publication. In this Letter, we concentrate on phantom data: MC simulation comparison of pixel intensity distribution statistics, with only a few illustrative Gamma function fits.

All data analysis was conducted using MATLAB (The MathWorks Inc., Natick, Massachusetts). To analyze the speckle intensity distributions for the simulated and experimental data, ROIs were selected to coincide with a region starting at 50 μm beneath the phantom surface, with a total axial depth of 350 μm and a width of 1 mm [see Fig. 1(a)]. The choice of ROI ensures that noise, which presumably has statistics different from that of OCT speckles, may minimally affect the resulting histograms. Histograms were generated from the envelope of the interference fringe signal (linear scale) for experimental and simulated data, with optimal histogram bin size determined according to Scott [17]. The Gamma probability distribution function,

$$f(x,\alpha,\beta) = \frac{1}{\Gamma(\alpha)}\beta^{\alpha}x^{\alpha-1}e^{-\beta x}, \tag{2}$$

Table 1. Optical Properties of Microsphere Phantoms at $\lambda = 1300$ nm

No.	d (μm)	Concentration $\times 10^9$ (mm^{-1})	Scat. Coeff. μ_s(mm^{-1})	Anisotropy g	Reduced Scat. Coeff. μ_s'(mm^{-1})
1	0.5	0.182	4.36	0.47	2.31
2	0.5	0.091	2.18	0.47	1.15
3	0.5	0.046	1.09	0.47	0.58
4	0.35	0.530	2.26	0.22	1.78
5	0.35	0.265	1.13	0.22	0.84
6	0.35	0.133	0.56	0.22	0.43

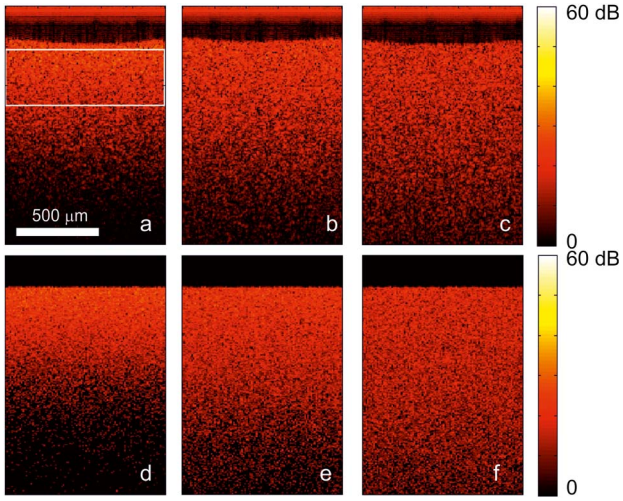

Fig. 1. Comparison of experimental (a)–(c) and simulated (d)–(f) OCT images for different concentrations of 0.5 μm diameter microspheres (samples 1–3, see Table 1). The solid box in (a) shows a typical ROI use in subsequent quantitative data analysis.

was then fitted to each histogram using a maximum likelihood estimation technique, as previously described [15,16], and the shape (α) and scale (β) parameters were subsequently extracted. Our study has shown that although the problem seems to be in general ill-posed (i.e., sensitive to missing or inaccurate data), our algorithm provides a relatively robust and unique set of parameters (α, β) to each curve, with smooth dependence on the optical properties of the samples.

Qualitative comparison of simulated and experimental OCT B-mode images from different suspensions of polystyrene microspheres are shown in Fig. 1. Good agreement between theory and experiment is noted by similar signal levels and similar signal decrease rates with depth, lending some credence to the validity of the Monte Carlo model in simulating the image speckle properties.

Some differences can be observed near the sample surface because it was considered to be ideally flat in the simulation, while exhibiting a slight curvature/meniscus in the experiments. However, this should not affect the speckle statistics in the subsurface ROI, as analyzed below.

To follow up the visual comparison of B-mode images, Fig. 2 displays simulation and experimental A-scans

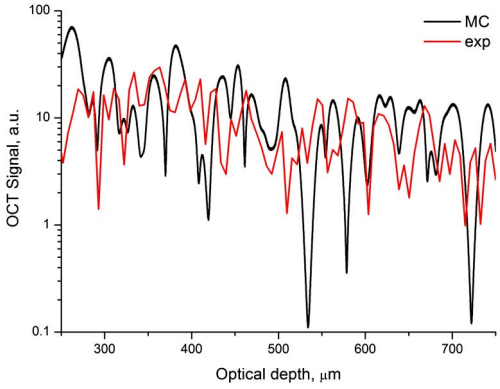

Fig. 2. Comparison of OCT signal (A-scans) for MC simulation and experiment of Sample 1.

(OCT signal envelopes) for Sample 1 (Table 1) within and below the subsurface ROI. Reasonable agreement between the simulated and measured A-scans is seen, with both showing similar depth decay trends and signal intensity variations indicative of local image texture (speckle). In fact, we do not expect precise agreement, given the random statistical nature of the speckle pattern formations. Differences between experimental and simulated results may also originate from the fact that the current simulation model does not accurately account for such experimental parameters as focusing of the incident beam and various noise sources, other conditions in the OCT detection apparatus.

In Figs. 3(a) and 3(b), the experimental OCT pixel intensity distributions are plotted for the 0.5 and 0.35 μm diameter microsphere samples, respectively, at three different concentrations (markers), and the corresponding Monte Carlo model predictions (lines). Overall similar trends are seen for both; the model captures the experimentally observed trend of the pixel intensity distributions shifting to lower signal values with decreasing scatterer concentration.

A side-by-side comparison of experiment and simulations, quantified with the Gamma distribution fits, is explored in Fig. 4. Representative Gamma distribution fits to histograms for one of the 0.5 μm diameter microsphere samples are shown in (a), and the Gamma parameters for all samples are plotted as a function of particle concentration for both sphere sizes in (b). From Fig. 4(a), it is once again evident that the experimental data and the Monte Carlo predictions agree well with each other, and that both are well described by the Gamma distribution fits.

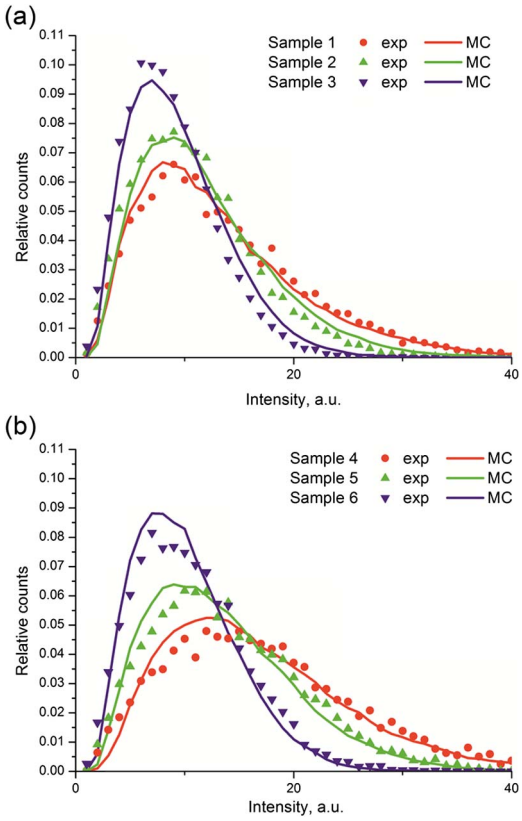

Fig. 3. Histograms for raw simulated (lines) and experimental (markers) OCT-images for (a) Samples 1–3 and (b) Samples 4–6.

The trends in the resulting fitting parameters are summarized in 4(b); while showing good agreement between fits to theory and to experiment, these are more challenging to interpret. As a starting point, we note that in ultrasound the shape parameter α has been related to the effective scatter number density (at least in low concentration suspensions of cells *in vitro* [16]); in light of this, its essentially concentration-independent behavior seen in the left panel of Fig. 4(b) is somewhat unexpected. Conversely, the scale parameter β is thought to be indicative of the mean signal amplitude and thus increases with increasing scatterer concentration and/or increase in the scattering strength (cross section) of the individual scatterer; both of these trends are borne out in the right panel of Fig. 4(b), with β increasing with microsphere concentration and being slightly larger for the higher-diameter microspheres. Further work is ongoing in understanding and interpreting the underlying sample properties potentially present in the Gamma distribution fitting parameters in the context of OCT.

In summary, the solid agreement between experimental and MC-simulated OCT signal statistics suggests that this MC simulation platform may prove useful in describing and modeling the OCT signal intensities and speckle patterns in biological tissues. Further, the development and interpretation of OCT Gamma fits may also shed light on the underlying scatterer characteristics that are contributing to the OCT signals.

In addition, the developed Monte Carlo code allows one to assess the signal contribution of the multiply scattered photons, which travel to the detector from outside the resolution volume [18]. Thus, one can specifically analyze the multiple scattering effects on speckle statistics. However, for the optical property ranges, ROI selections, and OCT system parameters reported in the present study, the contribution of the multiply scattered photons is likely minimal and such analysis is inapplicable.

We have previously demonstrated that statistical analysis of OCT signal intensity histograms can be used

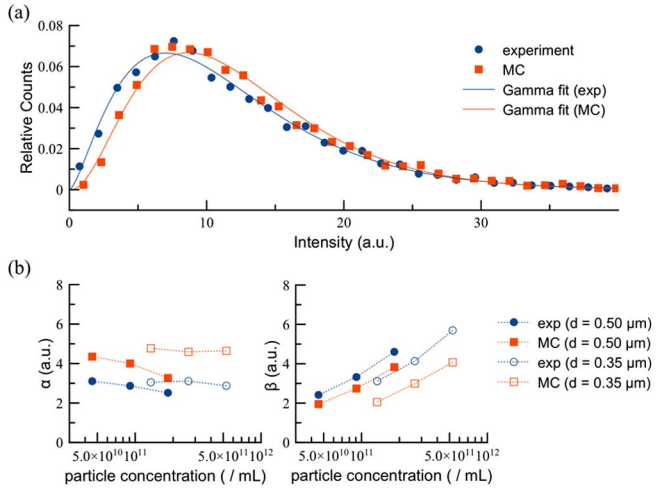

Fig. 4. (a) Representative histograms (markers) and Gamma distribution fits (lines) for Sample 1. (b) Gamma distribution parameters extracted from experimental and simulated signal intensity histograms. Shape α (left) and scale β (right) parameters are plotted as a function of particle concentration for both sized microspheres.

for differentiating between tissue types and for detecting cell death. However, further understanding of the effects of underlying tissue structure on OCT speckle statistics is required. An MC model has been developed to simulate the speckle statistics in OCT images from polystyrene microsphere phantoms with good agreement to experimental measurements. Further, the demonstrated Gamma distribution fits to speckle intensities may also provide physical insight into the underlying nature of the scattering medium contributing to the OCT signal. Both of these developments could play an important role in OCT signal analysis and tissue characterization efforts for diagnostic and treatment monitoring applications.

This study was supported the Canadian Institutes of Health Research (grant 126172), the Natural Sciences and Engineering Research Council of Canada (grant 216986-2012), the Russian Foundation for Basic Research (grant 13-02-97092), and the Ministry of Education and Science of the Russian Federation (grant 14.B25.31.0015).

References

1. T. R. Hillman, S. G. Adie, V. Seemann, J. J. Armstrong, S. L. Jacques, and D. D. Sampson, Opt. Lett. **31**, 190 (2006).
2. K. W. Gossage, T. S. Tkaczyk, J. J. Rodriguez, and J. K. Barton, J. Biomed. Opt. **8**, 570 (2003).
3. F. Bazant-Hegemark and N. Stone, J. Biomed. Opt. **13**, 034002 (2008).
4. F. Bazant-Hegemark and N. Stone, Lasers Med. Sci. **24**, 627 (2009).
5. P. B. Garcia-Allende, I. Amygdalos, H. Dhanapala, R. D. Goldin, G. B. Hanna, and D. S. Elson, Biomed. Opt. Express **2**, 2821 (2011).
6. Y. Yang, T. Wang, N. C. Biswal, X. Wang, M. Sanders, M. Brewer, and Q. Zhu, J. Biomed. Opt. **16**, 090504 (2011).
7. A. M. Pagnozzi, R. W. Kirk, B. F. Kennedy, D. D. Sampson, and R. A. McLaughlin, Biomed. Opt. Express **4**, 2383 (2013).
8. I. Meglinski, M. Kirillin, V. Kuzmin, and R. Myllyla, Opt. Lett. **33**, 1581 (2008).
9. M. Kirillin, I. Meglinski, V. Kuzmin, E. Sergeeva, and R. Myllyla, Opt. Express **18**, 21714 (2010).
10. G. Yao and L. V. Wang, Phys. Med. Biol. **44**, 2307 (1999).
11. M. Y. Kirillin, I. V. Meglinski, and A. V. Priezzhev, Quantum Electron. **36**, 247 (2006).
12. M. K. K. Leung, A. Mariampillai, B. A. Standish, K. K. C. Lee, N. R. Munce, A. Vitkin, and V. X. D. Yang, Opt. Lett. **34**, 2814 (2009).
13. Mie Scattering Calculator, http://omlc.ogi.edu/calc/mie_calc.html (accessed on 21.02.2014).
14. G. Farhat, V. X. D. Yang, G. J. Czarnota, and M. C. Kolios, J. Biomed. Opt. **16**, 026017 (2011).
15. A. A. Lindenmaier, L. Conroy, G. Farhat, R. S. Dacosta, C. Flueraru, and I. A. Vitkin, Opt. Lett. **38**, 1280 (2013).
16. A. S. Tunis, G. J. Czarnota, A. Giles, M. D. Sherar, J. W. Hunt, and M. C. Kolios, Ultrasound Med. Biol. **31**, 1041 (2005).
17. D. W. Scott, Biometrika **66**, 605 (1979).
18. M. Yu. Kirillin, A. V. Priezzhev, and R. Myllylä, Quantum Electron. **38**, 486 (2008).